ISSN 1027-5495. Functional Materials, 28, No.4 (2021), p. 729-736.
doi:https://doi.org/10.15407/fm28.04.729

Photocatalytic antibacterial performance of diatomite/nano-TiO_2 composite doped cement-based material

Gang Liao, Yuming He

Department of Traffic and Municipal Engineering, Sichuan College of Architectural Technology, 610399 Sichuan Chengdu, China

Received September 22, 2021

A diatomite/nano-TiO_2 (DNTC) composite was synthesized by a modified sol-gel method. The DNTCs were then added to a cement matrix to form cement-based photocatalytic materials (PCMs). The photocatalytic antibacterial ability of PCM was assessed by the degradation of Escherichia coli. It was shown that the photocatalytic activity of DNTC decreases with calcination temperature, and DNTC treated at 200°C exhibits high photocatalytic activity. The effect of PCM on the degradation of Escherichia coli increased with of DNTC, and the maximum degradation could reach 92.8 % when the DNTC mass fraction was 40 %. It has been found that DNTC can not only improve the dispersion of TiO_2, but also increase the concentration of Escherichia coli around the PCM, resulting in a synergistic e ffect of improving the photocatalytic an tibacterial ability of the PCM.

Keywords: photocatalytic sterilization, diatomite/nano-TiO_2 composite, photocatalytic cement-based material, photocatalytic activity.

Фотокаталітичні антибактеріальні властивості легованого матеріалу на основі цементу з композиції діатоміт/нано-TiO_2. *Gang Liao, Yuming He*

Синтезований композит діатоміт/нано-TiO2 (DNTC) модифіковано золь-гель методом. Потім DNTC було нанесено на цементну матрицю для створення фотокаталітичних матеріалів на основі цементу (ФКМ). Фотокаталітичну антибактеріальну здатність ФКМ оцінювали за розкладанням Escherichia coli. Показано, що фотокаталітична активність DNTC зменшується із збільшенням температури прожарювання, і DNTC, оброблена при 200°C, демонструє високу фотокаталітичну активність. Ступінь впливу ФКМ на розкладання Escherichia coli збільшується з дозою DNTC, а максимальне розкладання може досягати 92,8 %, коли маса DNTC складає 40 %. Виявлено, що DNTC може не тільки покращити дисперсію TiO_2, але також збільшити концентрацію Escherichia coli навколо ФКМ, що призводить до синергетичного ефекту покращення фотокаталітичної антибактеріальної здатності ФКМ.

Синтезирован композит диатомит/нано-TiO_2 (DNTC) модифицированным золь-гель методом. Затем DNTC наносили на цементную матрицу для образования фотокаталитических материалов на основе цемента (ФКМ). Фотокаталитическую антибактериальную способность ФКМ оценивали по разложению Escherichia coli. Показано, что фотокаталитическая активность DNTC снижается с увеличением температуры прокаливания, а DNTC, обработанные при 200°C, проявляют высокую фотокаталитическую активность. Степень воздействия ФКМ на разложение Escherichia coli увеличивалась с увеличением дозы DNTC, и максимальное разложение могло достигать 92,8 %, когда массовая доля DNTC составляла 40 %. Обнаружено, что DNTC может не только улучшить дисперсию TiO_2, но также увеличить концентрацию Escherichia coli вокруг ФКМ, что приводит к синергетическому эффекту улучшения фотокаталитической антибактериальной способности ФКМ.

1. Introduction

Currently, scientists around the world are paying great attention to the development of various methods of sterilization. Traditional sterilization methods using ozone [1, 2] and ClO_2 [3, 4] can effectively kill everyday pathogenic bacteria, but they release harmful byproducts such as endotoxin release.

Since photocatalysis of TiO_2 was found by Japanese scientists [5], TiO_2 has exhibited huge prospect in environment mitigation due to its nontoxicity, stability, and high photocatalytic activity [6, 7]. Tadashi Matsunaga et al. [8] first reported in 1985 that TiO_2/Pt could inactivate microbial cells. Lactobacillus acidophilus, Saccharomyces cerevisiae and Escherichia coli were all killed under the action of TiO_2/Pt catalyst coupled with the illumination of metal halide lamp for 60–120 min. Since then, more and more scholars began to study the photocatalytic antibacterial and sterilization properties of TiO_2 [9–14]. There are several main advantages of the TiO_2 photocatalyst as a sterilizing agent, namely, 1) the active oxidative species (AOPs) including ·OH and O_2^{-}· have a strong oxidation ability, which can decompose most pathogens; 2) it not only kills pathogenic bacteria, but also degrades the endotoxin released by bacteria without secondary pollution; 3) the driving force of photocatalytic reaction of TiO_2 is light illumination, and TiO_2 can work for a long time without any energy-supply. Although the sterilization properties of TiO_2 have been reported, the mechanism of photocatalytic sterilization has rarely been studied.

The aim of this paper is to improve the photocatalytic sterilization ability of photocatalytic cement-based materials (PCMs); and diatomite was chosen as the mid-carrier. Firstly, diatomite/nano-TiO_2 composites (DNTCs) were prepared, and then DNTCs were sprayed onto the surface of cement-based materials. Diatomite as the mid-carrier can improve the dispersion degree of TiO_2 and reduce the negative effect of hydration product of cement on TiO_2. Furthermore, diatomite has a special pore struc ture and can provide a synergetic effect on the photocatalytic reaction [15, 16]. Escherichia coli was chosen as the target pathogen to evaluate the photocatalytic disinfection ability of prepared PCMs. To characterize the microstructure of prepared samples, the methods of XRD, SEM-EDS, N_2 adsorption-desorption tests and UV-vis DRS were used.

2. Experimental

2.1. Raw materials

Conch brand P·O 42.5 cement was used in this work. Natural diatomite used in this study was provided by Sinopharm Chemical Reagent Co., Ltd. and its chemical composition is shown in Table 1. All reagents including Tetrabutyl orthotitanate (TBOT), nitric acid (HNO_3), and absolute ethyl alcohol (CH_3CH_2OH) were provided by Sinopharm Chemical Reagent Co., Ltd, China.

2.2 Sample preparation

2.2.1 Diatomite/nano-TiO_2 composites synthesis

At first, natural diatomite was washed by deionized water and dried at 100°C in a drying oven for 1 h to eliminate impurity. Then, 1 g HNO_3 was added into 100 g deionized water forming solution A, and 10 g TBOT was dropwise added into the solution A with stirring to obtain a milky white suspension. The suspension was heated in a water bath at 50° for 48 h to obtain a sol. Subsequently, 1 g diatomite was added into the TiO_2 sol. Then, the mixture was stirred for 1 h and then placed in a vacuum reactor with a negative pressure of 0.08 MPa for 4 h. Finally, the mixture was heated in a muffle furnace for 4 h at various temperatures (200°, 300°, 400°, 500°) to obtain diatomite/nano-TiO_2 composites (DNTCs). The samples were labeled as *n*-DNTC, where *n* denotes the final heating temperature, and DNTC represents diatomite/nano-TiO_2 composite, for example, 200-DNTC is the composite treated at 200°. For control experiment, pure TiO_2 was prepared through the same technical route.

2.2.2 DNTCs doped cement-based material preparation

8 g water was added into 20 g cement and mixed for a while, and then the fresh cement paste was casted in a plastic mold (F40 mm×10 mm). A certain amount of

Table 1. Chemical composition of natural diatomite, %

SiO_2	Al_2O_3	Na_2O	CaO	MgO	Fe_2O_3	SO_3	TiO_2	K_2O	P_2O_5
54.1	18.9	0.334	4.45	0.548	4.93	0.528	0.824	1.82	0.0996

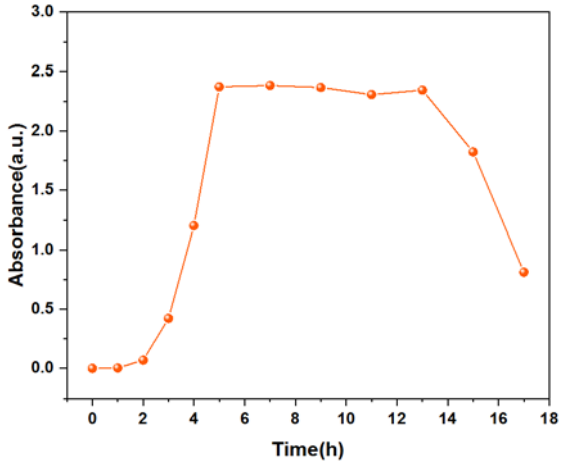

Fig. 1. Growth curve of Escherichia coli.

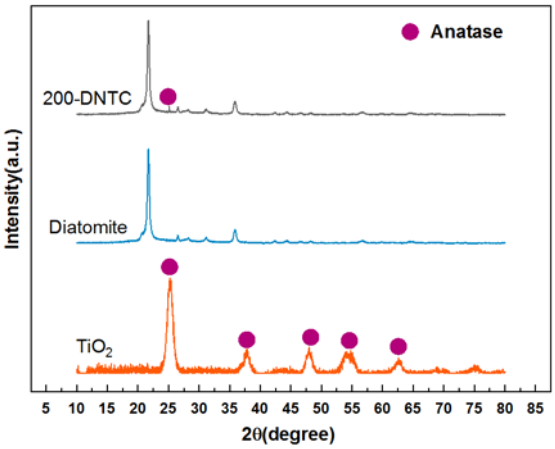

Fig. 2. X-ray diffraction patterns.

DNTC was sprayed onto the upper surface of cement paste before hardening. After 1 d, the sample was demolded and cured in a standard curing room (20±2°, *RH*≥95 %) for 28 d. The samples were labelled as *n*–*m*-PCM, where *n* is the heating temperature, *m*% is the mass ratio of DNTC to cement, and PCM represents a photocatalytic cement-based material, for instance, 200-20-PCM represents that DNTC was treated at 200° and the DNTC to cement ratio was 20 %.

X-ray diffraction was applied to characterize the crystal phase of as-prepared samples, and the diffraction angle (2θ) ranged from 10 deg to 80 deg with an interval of 0.02 deg at the speed of 4 deg·min–1. Scanning electronic microscopy (SEM) was used to observe the morphology of samples and energy dispersive spectroscopy (EDS) was used to confirm the micro-area element distribution. N2 adsorption-desorption tests were carried out to measure the BET specific surface area of samples. UV-vis DRS was used to measure the optical properties of DNTCs.

2.3 Photocatalytic sterilization test

2.3.1 Test of growth curve of Escherichia coli

Bacteria will experience four different growth periods, among which the bacteria in the logarithmic growth period have the best quality and the fastest growth speed. Thus, bacteria in the period of logarithmic growth are most suitable for experimentson photocatalytic degradation. Escherichia coli was inoculated with a medium solution containing 0.3 g beef extract, 1 g peptone, 0.5 g sodium chloride, and 100 mL water and then placed in a water bath at 37°C at a speed of 200 rpm. Absorbance of the medium solution was measured every 1h by a visible-spectrophotometer at the wavelength of 600 nm. The growth curve of Escherichia coli is shown in Fig. 1. It can be seen that Escherichia coli got into logarithmic growth period after 4 h.

2.3.2 Measurement of antibacterial activity of PCM

20 ml of the liquid medium of Escherichia coli sterilized at high temperature and 200 μL of the bacterial solution of Escherichia coli at the logarithmic phase were added into a beaker, and then the test PCM sample was immersed in the solution. Then after switching on ultraviolet light (75 W, main wavelength of 365 nm), 1ml of the Escherichia coli solution was sampled at an interval of 3 h. The absorbance of the sampled solution was measured by a visible-spectrophotometer at the wavelength of 600 nm. The degradation rate of Escherichia coli was calculated by the equation 1:

$$\xi = (C_0 - C_t)/C_0 \cdot 100\%, \qquad (1)$$

where C_0 is the initial absorbance of the Escherichia coli solution, and C_t is the absorbance of the Escherichia coli solution at time t. The whole experiment was operated in a sterile Table.

3. Results and discussion

3.1 Microstructure of diatomite/nano-TiO_2 composite

As shown in Fig. 2, for TiO_2 sample, diffraction peaks appeared at 2θ (25.305 deg, 37.799 deg, 48.038 deg, 55.062 deg, and 62.690 deg), which were in accordance with the characteristic peaks of anatase in PDF#73-1764. In general, anatase has the highest photocatalytic activity of all TiO_2 phases. This suggested that the modified sol-gel method used in this study promoted anatase formation through TBOT hydrolysis

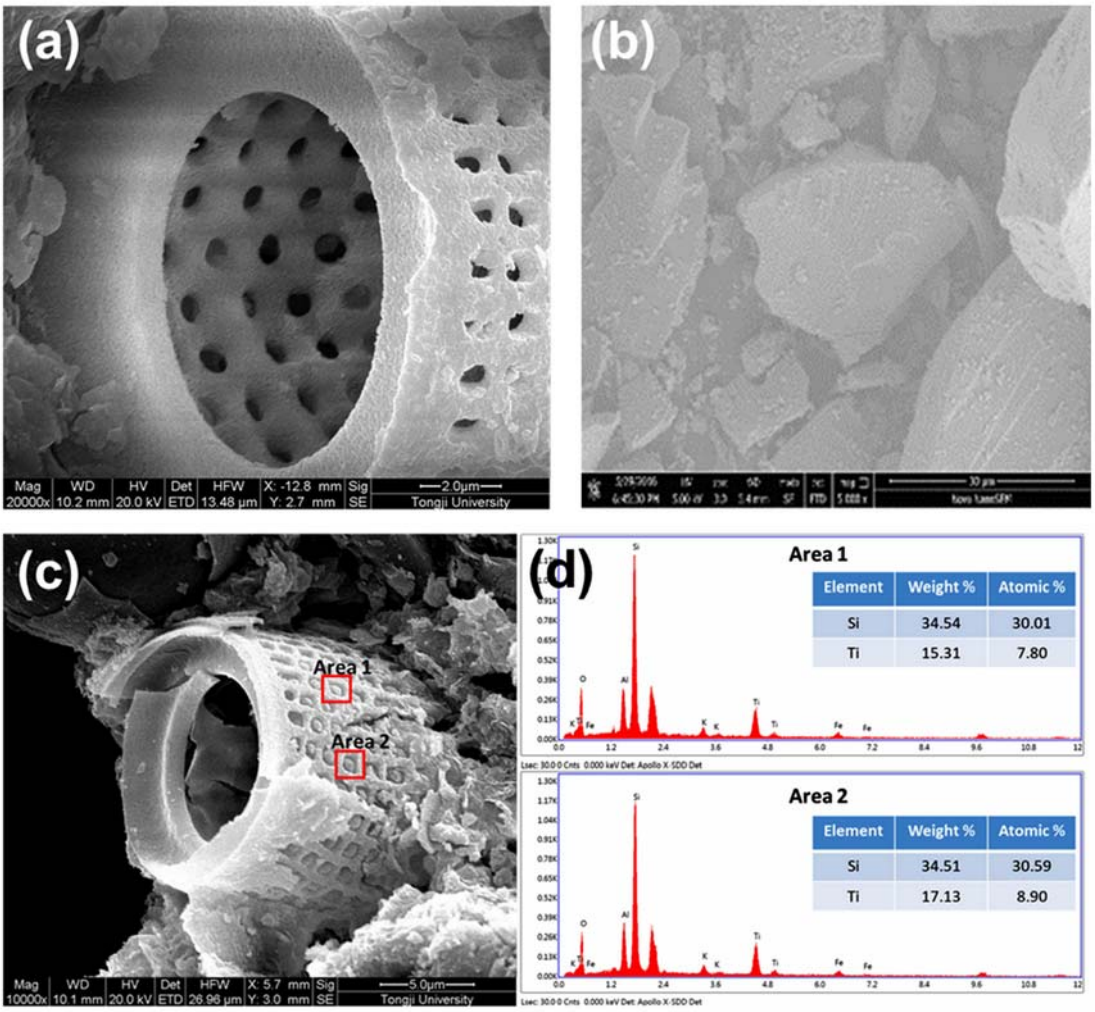

Fig 3. SEM images of (a) diatomite, (b) TiO2, and (c) 200-DNTC; (d) EDS

and hydrothermal treatment. It can be concluded that the diatomite/TiO_2 composite based on this method will possess excellent photocatalytic performance. In the diatomite sample, diatomite was amorphous, so only characteristic peaks of quartz were observed, indicating diatomite was doped with quartz. For 200-DNTC sample, the main crystal phase was still quartz, indicating that the structure of diatomite was stable even subjected to thermal treatment. This is significant for practical application in terms of the durability of the photocatalyst. It should be noted that a weak diffraction peak was detected at 2θ (25.305 deg) in the diffraction pattern of 200-DNTC, which corresponded to the strongest diffraction peak of anatase, thus proving that TiO_2 was successfully loaded on diatomite. Only one peak of anatase was observed due to the small addition of TiO_2. Another reason is that the TiO_2 crystal grain size in 200-DNTC was about 10 nm according to Scherrer's equation, so the intensity was too weak to be detected by XRD [17].

The morphology of all the samples was revealed by SEM. Fig. 3a shows the characteristic pore structure of diatomite, and the pores are regularly arranged without impurity. This pore structure is an ideal path for mass transfer and light transmitting. In addition, diatomite has a large surface area, which allows it to be used as a sorbent for pollutant molecules and a carrier for photocatalysts. Fig. 3b shows the SEM image of TiO_2 synthesized by the sol-gel method. It can be seen that TiO_2 is aggregated into blocks of several micrometers after thermal treatment and the nano-structure of TiO_2 is not observed. This indicates that if nano-TiO_2 particles are not dispersed well and firmly bonded with carriers, they tend to aggregate under thermal treatment, thus generating a dense structure and reducing

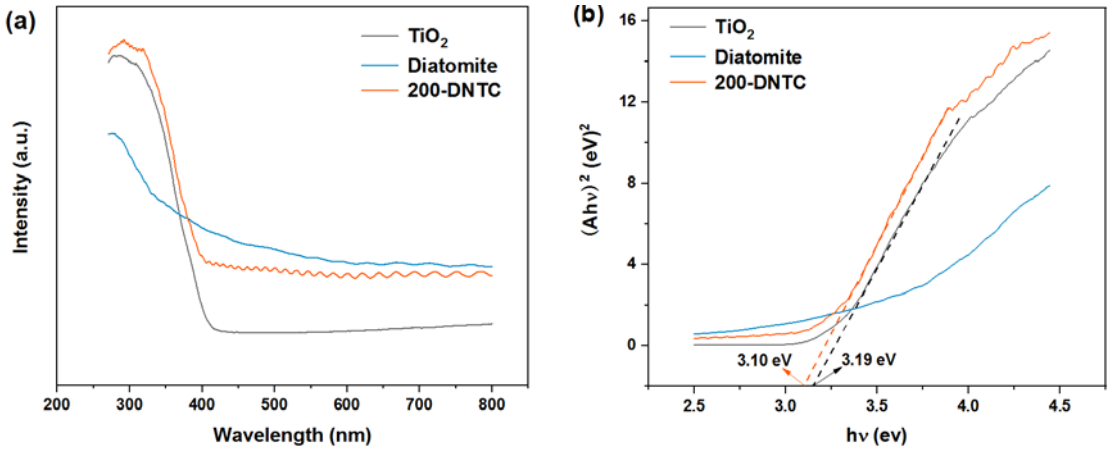

Fig 4. (a) UV-vis diffusive reflectance spectra; (b) Plots of (Ahn)2 vs. hnfor diatomite, TiO2 and 200-DNTC.

photocatalytic active sites. From this point of view, diatomite is an ideal carrier for TiO_2 due to its porous structure and large surface area. Also, diatomite may contribute to reduce the aggregation of TiO_2, thus increasing its dispersion degree. Furthermore, studies [15, 16] reported that there are abundant active radicals like –OH on the surface of diatomite, which can interact with TiO_2 and form chemical bonds. Thus, there are two positive effects, namely, 1) an increase in the bond strength between TiO_2 and diatomite; 2) construction of a path for the transfer of charge carriers. As shown in Fig. 3c, the morphology of 200-DNTC did not change after loading TiO_2, indicating that the loading amount was small and the dispersion degree of TiO_2 was high. The role of diatomite in the forming of TiO_2 can be described in detail as follows. After the hydrolysis of TBOT, TiO_2 exists as an intermediate with surface –OH in the sol. Upon heating, these intermediates will aggregate by dehydration in the absence of diatomite. However, when diatomite was added to the TiO_2 sol, a porous structure of diatomite interacted with the TiO_2 intermediate under the action of surface charge especially the surface –OH reacted with the intermediate by dehydration condensation, thus reducing the aggregation of TiO_2 and fixing nano-TiO_2 particles on the surface of diatomite by Ti–O–Si. From the EDS results in Fig. 3d, it can be seen that the content of the element Ti was almost the same in different regions, which suggests that TiO_2 was homogeneously dispersed on diatomite.

The BET specific surface area (S_{BET}), pore size, and pore volume data are presented in Table 2. It can be seen that SBET value of diatomite was relatively high up to 17.125 m^2/g, which was in accordance with the SEM results. After calcination, S_{BET} of TiO_2 decreased to 36.629 m^2/g, but it was still higher than that of diatomite. After loading TiO_2 on diatomite, S_{BET} of 200-DNTC increased a little up to 22.436 m^2/g, indicating that a TiO_2 nano-structure was constructed on the surface on diatomite and the porosity of the composite increased. In general, the structure with high S_{BET} can facilitate adsorption, desorption and diffusion of reactants and products in the photocatalytic process, so the DNTC synthesized in this study may have high photocatalytic activity.

Fig. 4 presents the optical properties of diatomite, TiO_2 and 200-DNTC. The absorbance of diatomite gradually decreased with wavelength, but did not show the typical absorption property of semiconductor due to no charge carrier excitation. For TiO_2 and

Table 2. Summary of surface characteristics of diatomite, TiO_2, and 200-DNTC

Sample	BET specific surface area, m^2/g[a]	Pore diameter, nm	Pore volume, cm^3/g[b]
Diatomite	17.125	12.564	0.059
TiO_2	32.629	5.853	0.107
200-DNTC	22.436	8.034	0.039

[a] Specific surface area measured using multi-point BET method.
[b] Pore diameter calculated from the desorption isotherm of BJH model.

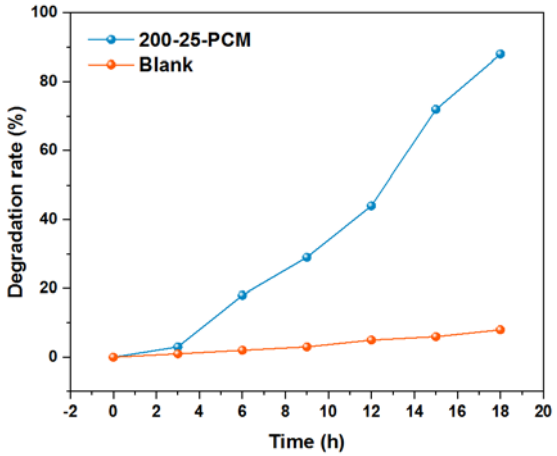

Fig. 5. Photocatalytic degradation rate of 200-25-PCM towards Escherichia coli.

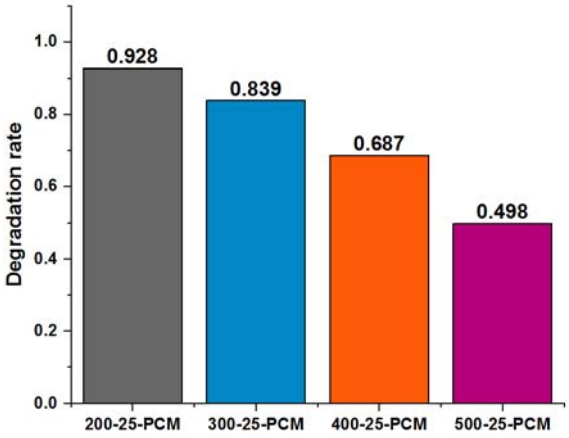

Fig. 6. Effect of temperature on degradation rate.

200-DNTC, there is a dramatic decline of absorbance in the range of 300–400 nm, indicating that both TiO_2 and 200-DNTC can absorb UV-light by generating hole-electron pairs; and TiO_2 endowed 200-DNTC with similar optical properties. However, the absorption edge of 200-DNTC is clearly shifted towards visible light compared to TiO_2, and the band gap of 200-DNTC (3.10 eV) was lower than that of P25 (3.19 eV) according to the Tauc plot method [18], which promotes the absorption of visible light. This may be explained by the interaction between TiO_2 and diatomite, which affected the band structure of TiO_2 and changed the migration behavior of charge carriers.

3.2 Photocatalytic degradation of Escherichia coli

Fig. 5a shows the photocatalytic degradation rate of Escherichia coli using 200-25-PCM. It can be seen that the for 200-25-PCM sample, the degradation rate increased with irradiation time, but for the blank sample, the concentration of Escherichia coli had a slight decline and nearly kept constant. This indicated that UV-light can only kill a small amount of Escherichia coli, while the photocatalyst was effective in eliminating Escherichia coli. The research [19] show that AOPs play the dominate role in inactivation of Escherichia coli. In detail, AOPs first attack the cell membrane of Escherichia coli by decomposing the LPS bilayer, phospholipid layer, and skin glycan (GN) la yer etc. and then degrade the metabolite or other left substances. It can be observed that the slope of the degradation curve increased with time, suggesting that the photocatalytic degradation reaction was inversely proportional to the concentration of Escherichia coli. This can be explained by the relationship between the quantity of AOPs and the concentration of Escherichia coli. Generally, the number of AOPs generated by TiO_2 is a constant under identical UV-irradiation. At the initial stage of reaction, the number of Escherichia coli was larger than that of AOPs, and moreover, the UV-light transmittance was very low at high concentration of Escherichia coli, thus generating less AOPs, so the reaction rate was low. With Escherichia coli degraded by AOPs, the number of AOPs was larger than that of Escherichi a coli and the UV-irradiation became stronger, and, as a result, the photocatalytic degradation rate increased.

Fig. 6 shows the influence of calcination temperature on the photocatalytic degradation rate towards Escherichia coli within 18 h. The degradation rate was the highest at 200° (92.8 %), but it gradually decreased with the calcination temperature. When temperature reached 500°, the degradation rate was lowest (only 49.8 %), which almost decreased by 50 %. It suggested that the PCM doped with 200-DNTC has the greatest photocatalytic activity. Although calcination is useful to some extent for the combination of TiO_2 with diatomite, however, high temperature will lead to the aggregation of nano-TiO_2, thus reducing the surface area and the number of active sites. Furthermore, the crystalline size of the TiO_2 increased with temperature, resulting in the redshift of optical energy gap, and consequently the redox potential of charge carriers became lower, and the activity of the catalyst decreased [6].

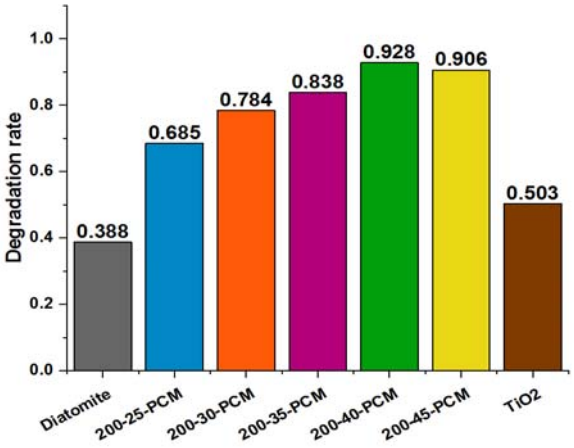

Fig. 7. Effect of 200-DNTC content on degradation rate.

Fig. 7 presents the degradation rate for PCM doped with different dosage of 200-DNTC. It's clear that the degradation rate increased with the content of 200-DNTC. When the content of 200-DNTC was 40 %, the degradation rate reached the highest value of 92.8 %, and upon exceeding 40 %, degradation rate started to decline. The reason was that the surface area of the cement matrix was limited; when the content of 200-DNTC was high, DNTC would overlapped with each other so that some of them cannot be irradiated by UV-light, and even worse, some DNTC would peel from the cement substrate, as a result the photocatalytic efficiency decreased. It can be also seen that PCM doped with diatomite can remove 38.8 % of Escherichia coli due the adsorption effect. The same mass of pure TiO_2 was added to PCM and its degradation rate was only 50.3 %. It's interesting that the degradation rate for the sum of diatomite and TiO_2 was 89.1 %, which was lower than that of 200-40-PCM (92.8 %). This indicates that there was a synergetic effect after TiO_2 was loaded on diatomite. Diatomite not only improved the dispersion degree of TiO_2, but also increased the concentration of Escherichia coli around TiO_2 through a strong adsorption effect.

The results of the repeated degradation experiment are shown in Fig. 8. The degradation rate at first cycle reached up to 92.8 % within 18 h. However, the degradation rate decreased slightly from the second cycle. When the tests were repeated for 3 times, the third degradation rate was still 85.8 %. Overall, the stability of PCM doped with DNTC was excellent. The slight decline in degradation rate was probably due to the occupation of TiO_2 active sites by the residue. And the photoc atalytic activity can be recovered by washing or heating PCM.

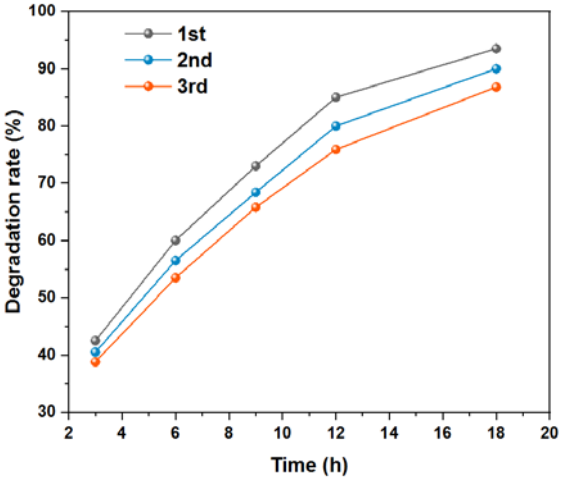

Fig. 8. Cycling degradation rate of 200-40-PCM towards Escherichia coli.

4. Conclusions

To sum up, the diatomite/nano-TiO_2 composite was successfully synthesized via a modified sol-gel method. SEM images and BET results showed that diatomite had a porous structure with a large specific surface area. XRD and EDS results confirmed that nano-TiO_2 particles were homogeneously distributed on the surface of diatomite. The photocatalytic activity of DNTC decreased with calcination temperature due to a decrease in the specific surface area of TiO_2. The degradation rate of Escherichia coli using PCM increased with the dosage of DNTC, and the highest value reached 92.8 % within 18 h, which was higher than that of the sum of diatomite and TiO_2. The synergetic effect of diatomite and TiO_2 was noticeable. After 3 times repeated experiments, the degradation rate still maintained 85.8 %, proving that the stability and durability of the as-prepared PCM was excellent.

Funding information: This research was funded by Deyang Science and Technology Program (No. 2020SZZ047, No. 2019SZ083).

References

1. I.Zucker, Y.Lester, J.Alter et al., *Environ. Chem. Lett.*, **19**, 1779 (2021).
2. D.Towle, V.Baker, C.Schramm, M.O'Brien et al., *Pediatr. Pulm.*, **53**, 599 (2018).
3. T.L.Chen, Y.H.Chen, Y.L.Zhao, P.C.Chiang, *Aerosol Air Qual. Res.*, **20**, 2289 (2020).
4. Q.X.Zhong, A.Carratala, S.Nazarov et al., *Environ. Sci. Tech.*, **50**, 13520 (2016).
5. A.Fujishima, K.Honda, *Nature*, **238**, 37 (1972).
6. Q.Guo, C.Zhou, Z.Ma, X.Yang, *Adv. Mater.*, **31**, 1901 (2019).

7. A.Fujishima, X.Zhang, D.A.Tryk, *Surf. Sci. Rep.*, **63**, 515 (2008).
8. T.Matsunaga, R.Tomoda, T.Nakajima, H.Wake, *Fems. Microbiol. Lett.*, **29**, 211 (1985).
9. H.N.Pantaroto, A.P.Ricomini, M.M.Bertolini et al., *Dent. Mater.*, **34**, 182 (2018).
10. H.M.Yadav, J.S.Kim, S.H.Pawar, *Korean J. Chem. Eng.*, **33**, 1989 (2016).
11. S.Senthilkumar, M.Ashok, L.Kashinath et al., *Smart. Sci.*, **6**, 1 (2018).
12. Z.H.Jing, X.E.Liu, Y.Du et al., *Front. Mate. Sci.*, **14**, 1 (2020).
13. T.Sato, M.Taya, *Biochem. Eng. J.*, **30**, 199 (2006).
14. W.C.Oh, A.R.Jung, W.B.Ko, *Mater. Sci. Eng. C-Bio. Supram. System*, **29**, 1338 (2009).
15. K.J.Hsien, W.T.Tsai, T.Y.Su, *J. Sol-Gel Sci. Technol.*, **51**, 63 (2009).
16. X.F.Liu, Y.G.He, B.B.Yang et al., *Catalysts*, 10 (2020).
17. I.Jansson, S.Suarez, F.J.Garcia-Garcia, B.Sanchez, *Appl. Catal. B-Environ.*, **178**, 100 (2015).
18. J.Tauc, R.Grigorovici, A.Vancu, *Physica. Status Solidi (b)*, **15**, 627 (1966).
19. J.H.Yan, H.Chen, L.Zhang, J.Z.Jiang, *Chin. J. Chem.*, **29**, 1133 (2011).